

RSC Advances



This is an *Accepted Manuscript*, which has been through the Royal Society of Chemistry peer review process and has been accepted for publication.

Accepted Manuscripts are published online shortly after acceptance, before technical editing, formatting and proof reading. Using this free service, authors can make their results available to the community, in citable form, before we publish the edited article. This *Accepted Manuscript* will be replaced by the edited, formatted and paginated article as soon as this is available.

You can find more information about *Accepted Manuscripts* in the [Information for Authors](#).

Please note that technical editing may introduce minor changes to the text and/or graphics, which may alter content. The journal's standard [Terms & Conditions](#) and the [Ethical guidelines](#) still apply. In no event shall the Royal Society of Chemistry be held responsible for any errors or omissions in this *Accepted Manuscript* or any consequences arising from the use of any information it contains.

ARTICLE

Natural, biodegradable and flexible egg shell membranes as separators for lithium-ion batteries

Cite this: DOI: 10.1039/x0xx00000x

M. Raja, A. Manuel Stephan*

Received 00th January 2012,

Accepted 00th January 2012

DOI: 10.1039/x0xx00000x

www.rsc.org/

Flexible egg shell membranes (ESM) were obtained from chick eggs after treating with hydrochloric acid. The ESMs were subjected to scanning electron microscopy (SEM), thermogravimetric (TG) and wettability analyses. The morphological studies revealed that the membranes possessed uniform porosity and were of micron sized. The ESM was also found to be thermally stable above 230 °C. The electrochemical properties such as ionic conductivity, lithium transport number (Li_t^+) and compatibility of the membrane upon activation in 1M LiPF_6 in EC:DMC(1:1 v/v) were analyzed. Finally, a 2032-type coin cell composed of Li/ESM/ LiFePO_4 was assembled and its cycling profile was also analyzed at different C-rates.

Introduction

The demand for energy storage devices with high energy and power densities in order to reduce the CO_2 emissions and dependence on definite resources on fossil fuels has prompted researchers to find alternative energy resources [1-2]. The state-of-art lithium-ion batteries are composed of a carbonaceous anode and lithium transition metal oxide cathode separated by a polyolefin separator soaked in a non-aqueous liquid electrolyte (1M LiPF_6 in EC:DEC 1:1v/v) [3]. However, the safety aspect of the present lithium-ion batteries is a frightening challenge for the users [4]. The separator is an important component which prevents the physical contact between the cathode and anode (precludes short-circuiting) while rapidly permitting the Li^+ ions for cycling. The membranes properties such as porosity, tortuosity, shrinkage, wettability and ionic conductivity influence the cycling performance of the batteries. Although, polyolefin membranes are widely used as separators in the commercially available lithium-ion batteries, they have several disadvantages such as low porosity (about 40%), poor wettability and unidirectional mechanical integrity [5]. Above all, it is thermally stable up to 135 °C. Therefore, membranes with enhanced thermal stability and good wettability in organic liquid electrolytes are highly desirable to guarantee safe and reliable lithium-ion battery systems [6]. Numerous reports are available on the preparation and characterization of porous membranes with high porosity and mechanical integrity for lithium-ion batteries [7,8]. Phase inversion method has been widely employed for the preparation of porous membranes; however, these membranes suffer from poor rate-capability [9-10]. Electrospun nanofibre-based nonwoven membranes have been very attractive in the recent years [11-12]. However, the lower mechanical integrity of the highly porous membrane hampers it from practical applications [13]. Intensively, numerous attempts have been made to employ ceramic membranes for lithium-ion batteries [14-17].

In the recent years, bio-sourced materials are widely used to enhance the electrochemical properties of energy storage

devices. Manuel Stephan et al., employed biomass derived carbonaceous materials from banana fibers for lithium-ion batteries [18]. In a similar way, the performance of supercapacitor was also studied [19]. Nanoscale microfibrillated cellulose (NMFC) was introduced into a light-cured polymeric matrix to as a quasi-solid electrolyte for the next-generation of bio-based dye-sensitized solar cells by Annalisa and co-workers [20]. According to the authors, the NMFC- added polymeric membrane promoted the sunlight efficiencies as high as 8.25% and also the long-term stability and excellent durability. Dyatkin et al., [21] have successfully demonstrated the performance of a green supercapacitor composed of environmental-friendly materials with porous acetate cellulose ester membranes which exhibited high gravimetric capacitances with low resistance values.

Very recently, egg shell membranes (ESM) have been widely employed as a template for the synthesis of ZrO_2 [22], TiO_2 [23] and Co_3O_4 [24] and precursors for carbonaceous materials [25]. It has also been used as separator for supercapacitors in aqueous medium [26].

Naturally, the avian eggshells are composed of layered organization of calcified shell and organic collagen types I, V, and X, and glycosaminoglycan [27]. It is the most abundant material in the biosphere which is non-toxic, environmentally benign and very cheap. Egg shells are hierarchically architected with three layers namely, outer shell membrane, inner shell membrane, and limiting membrane that surrounds the egg white [28]. The outer shell membrane, which can be easily isolated from egg shells can be used as separator for energy devices.

Even though numerous reports are available on polymeric and ceramic based membranes, as separators for lithium-ion batteries, studies based on naturally available and biodegradable porous membranes are very scanty and are truly interesting due to their cost effectiveness. So far to the best of our knowledge no attempt has been made to employ egg shell membranes as separator for lithium-ion batteries. In the present

work, the obtained ESMs were thoroughly characterized from the morphological and physico-chemical points of view.

Experimental

Preparation of membrane

Membranes were removed from the egg shells as reported earlier [27,28]. Briefly, eggs were gently broken and emptied via the blunt end and the egg shells were washed with water. Subsequently, the inner shell membrane and the limiting membrane were manually removed. The remaining egg shells were rinsed in 1M HCl to dissolve the CaCO₃, leaving the organic outer shell membrane. After the outer shell membrane was washed with water thoroughly, and was further purified by 2-propanol in order to remove the microorganism from the fine pores of the membrane. The morphology of the ESM was examined by scanning electron microscopy (SEM, Vega3, Tescan) under a vacuum condition (10⁻¹ Pa) after coating gold on one side of the membrane. Thermal stability of the egg shell membrane was analyzed by taking TG-traces in the ranges of 20°C to 600°C in N₂ atmosphere. The dimensional stability of the ESM was determined by storing both ESM and Celgard membrane at 125 °C in an oven for 1h. The contact angle of the ESM with non-aqueous liquid electrolyte was measured by a contact angle tester (Data Physics OCA35, Germany). The ionic conductivity of the membrane, sandwiched between two stainless steel blocking electrodes (1 cm² area) was measured using an electrochemical impedance analyzer (IM6-Bio Analytical Systems) between the frequency ranges from 1MHz to 50 mHz for various temperatures. In order to investigate the compatibility of the ceramic membrane with lithium metal anode, a symmetric non-blocking cell (Li/ESM/Li) was assembled and the time dependence of the impedance was analyzed at 25 °C. The lithium transference number was calculated by the method proposed by Vincent and co-workers [29].

$$Li^+_{t} = \frac{I_{ss}(V - I_0 R_0)}{I_0(V - I_{ss} R_{ss})} \dots \dots \dots (1)$$

The Li/CPE/Li cell was polarized by a dc pulse of 10mv. Time evolution of the resulting current flow was then followed. The initial (I₀) and steady state (I_{ss}) values of current flowing through the cell during the polarization were measured. R₀ and R_{ss} represent the resistance values before and after the perturbation of the system. Impedance spectra were made before and after perturbation.

The electrochemical stability window was measured by a sweep voltammetry in a two stainless steel electrode -poly(propylene) symmetric cell. Acetylene black coated on an aluminum current collector and lithium metal were used as electrodes and activated ESM was used as electrolyte. The potential scan range was from OCV to 5.5 V vs. Li and potential scan rate was 0.1 mV S⁻¹ [30]. The thermal shut-down property of the membranes was measured as described by Zhang [31].

A 2032-type coin cell was assembled in order to determine the cyclability of egg shell membrane. It was carried out by galvanostatic charge/discharge cycling at ambient temperature (current regimes from 0.1C to 1C) with an Arbin Instrument Testing System model BT-2000, setting the cut-off potentials between 2.50–4.00 V vs. Li/Li⁺. The composite cathode was prepared by blending LiFePO₄ as active material with

acetylene black carbon and PVdF-HFP as binder [32]. The ESM was soaked in the liquid electrolyte (1.0 M lithium hexafluorophosphate (LiPF₆, Aldrich) solution in a 1:1 v/v mixture of ethylene carbonate (EC, Fluka) and diethyl carbonate (DEC, Aldrich, USA). All preparations were performed in an argon-filled glove box (MBraun, Germany) having a humidity content below 1 ppm. The LiFePO₄/C cathode material was synthesized in the form of nanostructured powder through a mild hydrothermal procedure previously described in detail [30,32,33]. The lithium metal foil (Aldrich, USA) was used as anode.

Results and Discussions

Figure 1 (a & b) shows the surface morphology of ESM's for two different magnifications. The SEM images revealed that the surface has a rough morphology and the average pore size is 1- 5 microns. The interconnected pores are expected to entrap huge amount of non-aqueous electrolytes upon soaking the membrane into it.

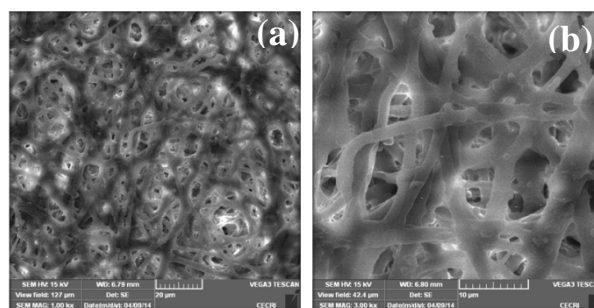


Fig.1. SEM images of ESM at different magnifications (a) x 1000 (b) x 3000

In order to ascertain the thermal stability of ESM the thermogravimetric (TG) analysis was made between 25 and 600 °C. Generally, the weight loss of ESM takes place in three –steps as depicted in Figure 2. The weight loss seen at around 50-100 °C is attributed to the removal of water and moisture from the membrane. The degradation of collagen and glycon chains decomposes between 220 and 400 °C [27].

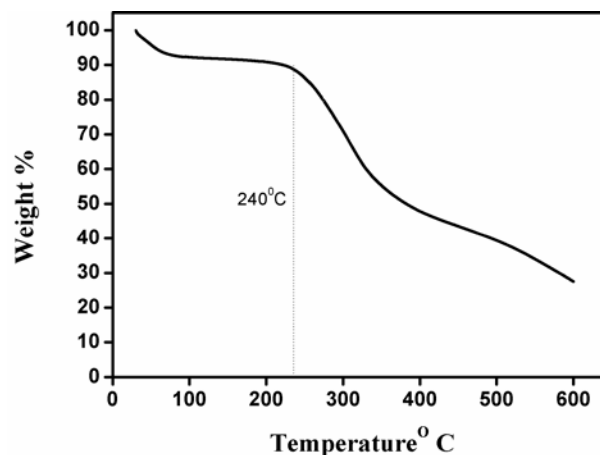


Fig.2. Thermogravimetric traces of ESM

The irreversible decomposition starts at 240 °C. The degradation of membrane matrix takes place between 400 and 600 °C which is in accordance with the earlier reports [25, 27,27]. The shut down temperature for ESM and Celgard membranes is found as 205 and 160 °C respectively.

Table. 1. The physical properties of ESM and Celgard

Membrane Properties	ESM	Celgard 2400 [^]
Porosity	60%	41%
Electrolyte Uptake	81%	60%
Li-ion transport number	0.47	0.44
Contact angle	65°	35°
Shutdown temperature	205°C	160°C

membranes obtained at our laboratory conditions.

Figure 3 shows the photograph of commercially available Celgard 2400 membrane and ESM before and after heat treatment (storing both membranes at 125 °C for one hour). It is clear from the photograph that ESM is dimensionally more stable than the commercially available membrane.

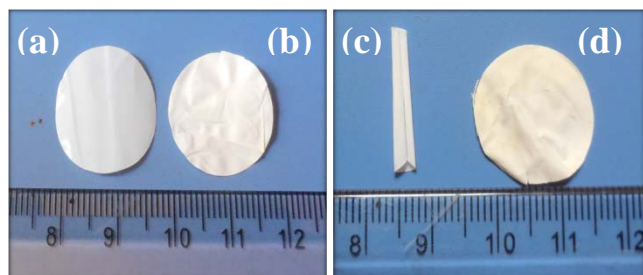


Fig. 3. Photographs of ESM and Celgard membranes before and after heat treatment at 125°C. (a) Celgard (b) ESM (c) Celgard (d) ESM

The percentage of porosity of the membrane was determined using the equation (2) after soaking the ceramic membrane in n-butanol;

$$P(\%) = [(M_1/\rho_1)/(M_1/\rho_1 + M_2/\rho_2)] \times 100 \text{ ----- (2)}$$

Where M_1 and M_2 denotes the masses of the dry ESM and n-butanol absorbed membrane respectively, while ρ_2 and ρ_1 represent the densities of the ESM and n-butanol, respectively. The porosity of the membrane was found to be 60 %. In the present study n-butanol was selected as its viscosity is very close to that of non-aqueous liquid electrolytes used for lithium-ion batteries [34-36]. The uptake of electrolyte solution was measured using equation (3)

$$\text{Uptake (\%)} = [(M - M_0)/M_0] \times 100 \text{ ----- (3)}$$

The uptake of the electrolyte was measured as 81%. Table 1 depicts the physical and electrochemical properties of both ESM and Celgard membrane.

The tortuosity of the membrane is the ratio of mean capillary length to thickness of the membrane which shed light on the pore blockage and average pore connectivity [5].

The tortuosity of the membrane was calculated by employing the formula (4); where σ_0 and σ represents the ionic conductivity of the liquid electrolyte and activated egg shell membrane (after swelling in the electrolyte) respectively. The “P” represents the porosity of the membrane.

$$T = [(\sigma/\sigma_0) \times P]^{1/2} \text{ -----(4)}$$

The tortuosity of the membrane was found to be 24.5

According to Zhang John and Arora [5], an ideal porous body with cylindrical and parallel pores represent a tortuosity factor equal to 1. The higher the value of tortuosity, is more the hindered system. However, higher tortuosity leads to better dendrite resistance at the same time it adversely increases separator resistance. In the present study the tortuosity of the membrane was found to be 24.5.

The wettability of a separator with liquid electrolyte plays a pivotal role in the electrochemical properties of a cell. The poor wettability of the separator enhances the cell resistance and thereby reduces the rate capability significantly [5,8,37]. The contact angle of Celgard and ESM was measured as 65° and 35° respectively as shown in Figure 4. For the ESM the droplet of the electrolyte promptly infiltrated in to the membrane and the contact angle is less than the Celgard membrane. The better wettability facilitates high uptake of electrolyte. The reduction in the value of contact angle is attributed to better capillary force of the pores into ESM and also close polarity between ESM and non-aqueous liquid electrolyte [37].

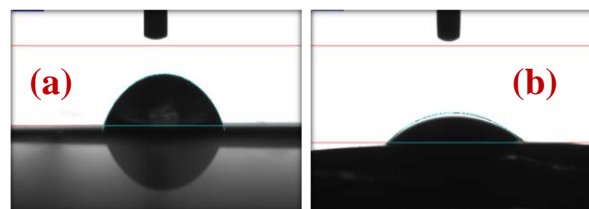


Fig.4. Contact angle images of (a) Celgard and (b) ESM with non-aqueous liquid electrolyte of 1M LiPF₆ EC+DEC (1:1 v/v).

The stress-strain profile of ESM and Celgard membranes are depicted in Figure 5. The tensile strength of Celgard membrane is 1.42 MPa with an elongation-at-break of 150%. On the other hand, the ESM exhibited a tensile strength of 1.12 MPa which is inferior to the value of Celgard membrane. A similar observation has been reported by Fan and Maier [38] where the authors reported the tensile studies on PEO-based electrolytes.

The ionic conductivity of ESM and Celgard membrane was measured for various temperatures by impedance spectroscopy and the Arrhenius behavior is depicted in Figure 6.

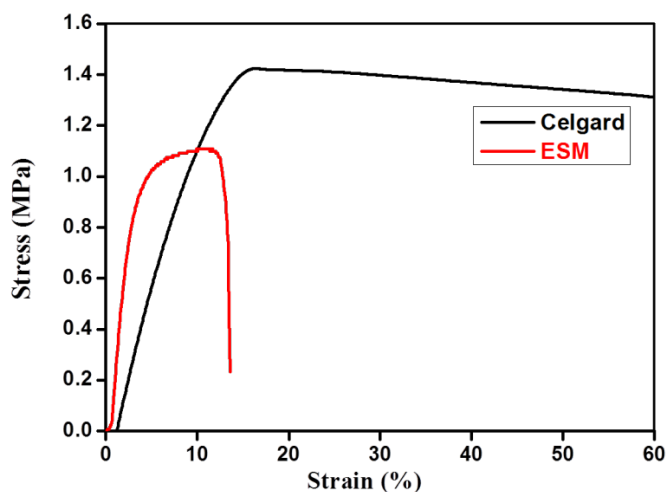


Fig. 5. The tensile strength of Celgard and ESM membrane

lithium electrode with the ESM [39]. The value of Li_t^+ has been calculated as 0.47 which is slightly higher (0.44) than that of the commercially available membrane [40].

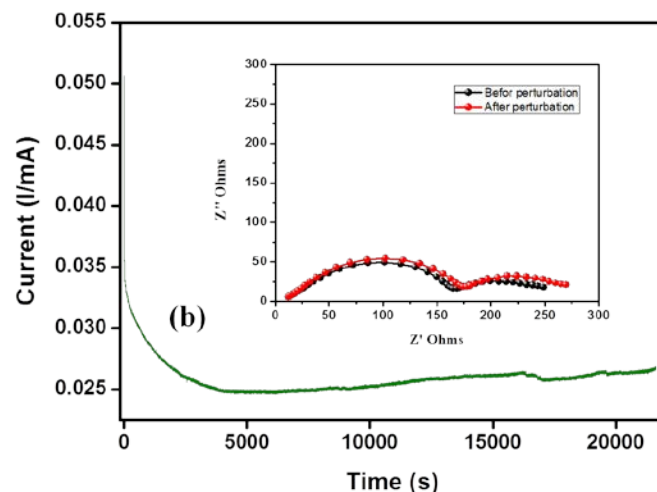
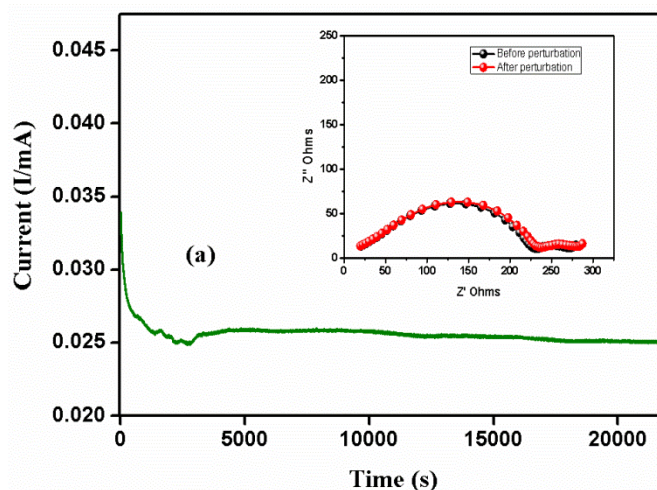


Fig. 7. The chronoamperometric profile for (a) ESM (b) Celgard membrane activated in non-aqueous liquid electrolyte of 1M LiPF_6 EC+DEC (1:1 v/v). Inset: Nyquist plot of symmetric cell before and after perturbation.

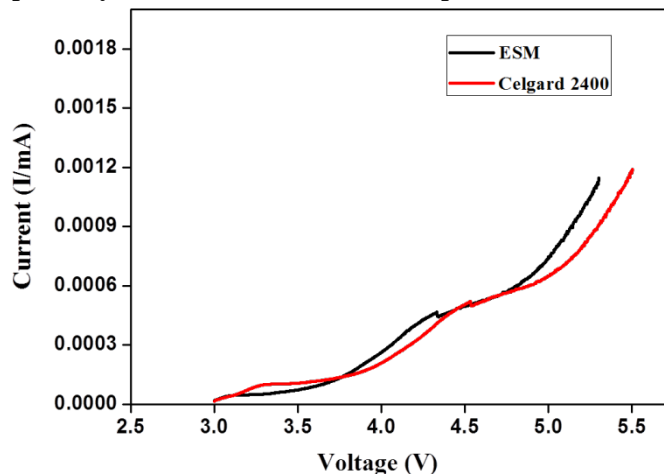


Fig. 8. Electrochemical stability window at room temperature for ESM and Celgard 2400 activated in non-aqueous liquid electrolyte of 1M LiPF_6 EC+DEC (1:1 v/v).

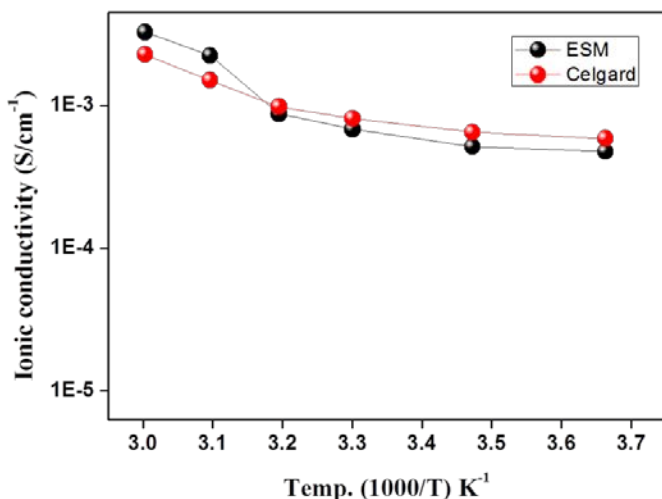


Fig. 6. Ionic conductivity vs. inverse temperature of ESM.

The ionic conductivity of Celgard membrane is slightly higher than that of ESM at lower temperatures however; the order of ionic conductivity is same for both membranes. The ESM membrane showed an ionic conductivity of the order of 10^{-4} S cm^{-1} at 30 °C. The ionic conductivity increases with the increase of temperature, resulting in the high value 1×10^{-3} S cm^{-1} at 50 °C. The activation energy was calculated as 1.32eV and 1.30 eV for ESM and Celgard membrane respectively.

The lithium transference number, Li_t^+ , is a key parameter which guarantees the performance and rate capability of lithium batteries for the applications in power tools [39]. As mentioned in the experimental section the lithium transference number was calculated using the equation (1) [16]. Fig. 7 (a & b) shows the chronoamperometric curve of ESM and Celgard membrane respectively. Insets show their corresponding Nyquist plots before and after perturbation. Apparently, both curves (before and after perturbation) overlap, indicating that there is no much difference between the initial R_0 and the final resistance R_{ss} of the two Li interfaces, which further confirms the stability of the

The electrochemical stability window which sheds light on the cycling reversibility of battery systems was evaluated for both ESM and Celgard membrane. Figure 8 illustrates the electrochemical stability window between 3.0 - 5.5V at ambient temperature. In the present study, for both membranes the decomposition of the electrolyte indicates an anodic breakdown voltage of approximately 4.8V vs. Li with low residual current [30]. This high voltage decomposition is certainly appreciable for practical applications.

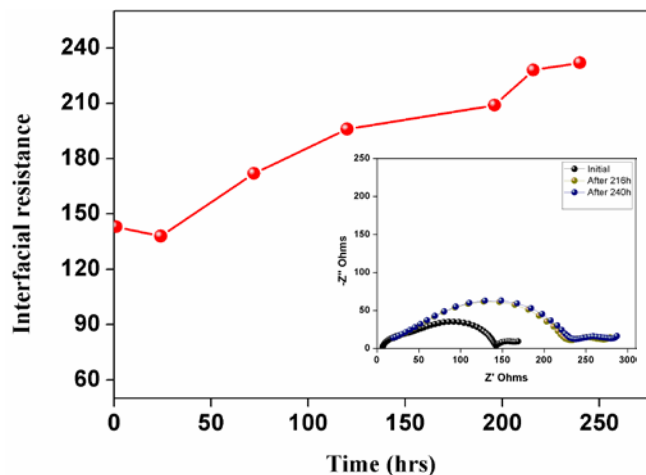


Fig.9. Variation of interfacial resistance R_i vs. time for the symmetric cell Li/ESM/Li at 25 °C. Inset: The Nyquist plot 9at different time interval

However, the current rises at a lower voltage, which is attributed to a sort of “passivation” and the reason for this behaviour is yet to be understood. A similar observation has been reported by Gerbaldi et al [30] where the authors reported the electrochemical properties of UV-cured methacrylic based gel polymer for lithium-ion batteries.

High ionic conductivity and appreciable transport number are although, desirable properties, which are not sufficient to guarantee membranes completely useful for practical applications. It is well known that the resistance of the cell is composed of the bulk resistance (R_b) of the electrolyte and the interfacial resistance (R_i) reflects the electrodes and electrolyte interfacial properties [41,42]. In order to analyze the interfacial properties of ESM with lithium metal anode the impedance response of the symmetric cell composed of Li/ESM/Li was monitored as a function of time under open circuit voltage conditions. Generally, the interfacial resistance are measured from the Cole–Cole impedance plots (shown as inset in figure 9) in which the large semi-circles represent a parallel combination of resistance (R_{film}) and capacitance associated with the passivation film on the Li electrode [41,42].

A small semicircle is due to the charge transfer resistance in parallel with the double layer capacitance. The intercept of the large semi-circle at high frequency on the Z-axis is mostly associated with the interfacial resistance “ R_i ” of the system. Figure 9 illustrates the variation of interfacial resistance of as a function of time for the symmetric cell comprising Li/ESM/Li. The value of R_i increases with time sharply which indicates the formation of the passivation layer on the surface of lithium. After 200 hours of storage the value of R_i remains same (less than 300 ohms) indicating that the ESM is stable towards

lithium metal anode. This is attributed to the porous nature of the membrane [43].

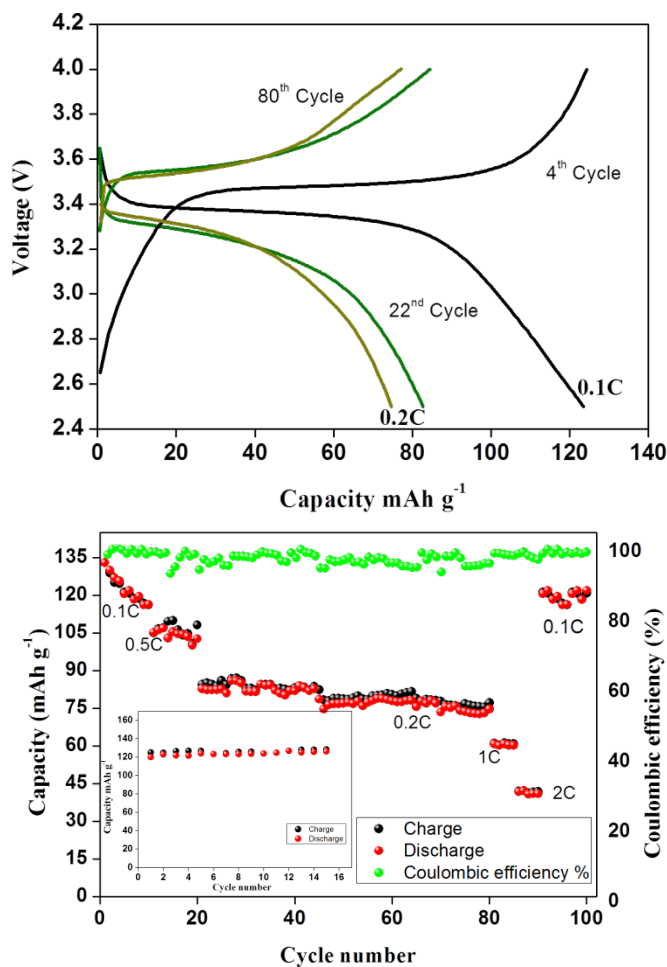


Fig.10 (a) Cycling profile of Li/ESM/LiFePO₄ cell. **(b)** Discharge capacity as a function of cycle number for the cell Li/ESM/LiFePO₄ for different current regimes. Inset Cycling profile of Celgard membrane at 0.1C-rate.

Figure 10 (a & b) shows the typical charge-discharge behaviour of Li/ESM/LiFePO₄ cell obtained at room temperature for different C-rates. In set figure shows the cycling profile of Celgard membrane at 0.1C-rate for a comparison. All curves show a typical and flat voltage plateaus at 3.45- 3.52 V vs. Li⁺ on charge and 3.38 and 3.30 V vs. Li on discharge and is due to the biphasic Li⁺ extraction/insertion mechanism of LiFePO₄ cathode. A small drop in voltage was observed from charge to discharge indicates the lower cell resistance value. This lower cell resistance is attributed to the better adhesion of the separator on both sides of the electrodes which may significantly contribute to reduce the interfacial resistance of the cell [38]. The discharge capacity as a function of cycle number of Li/ESM/LiFePO₄ for various C-rates viz., 0.1, 0.2, 0.5, 1 and 2 C. This cycling behaviour exhibits good capacity retention up to 100 cycles. In order to analyze the cycling

ability, the cell was allowed run for 60 cycles at 0.2C-rate. We do not find any discernible changes in the cycling profile and the fade in capacity per cycle was 0.1 mAh g⁻¹. Although, the cell exhibited low discharge capacity in the initial cycles, it delivered a stable cycling profile after 11th cycle. The cell delivered a discharge capacity of 133 mAhg⁻¹ in its first cycle and 116 mAhg⁻¹ at its 10 cycle indicating a fade in capacity of 1.7 mAh per cycle and is attributed to the formation cycles. However, in the subsequent cycles, a stable cycling is achieved with 99% Coulombic efficiency and is attributed to the improved interfacial property of the cell which was substantiated by impedance spectroscopic analysis by Gerbaldi et al [30].

An abrupt decrease in capacity was observed at 1C and 2C-rates. The reduction in the discharge capacity at higher current regime is a typical characteristic of LiFePO₄ material which is attributed to its low electronic conductivity and limited diffusion of Li⁺ ion into its structure that causes electrode polarization [44, 45]. Further, the declining discharge capacity at higher C-rates may be due to the solid electrolyte interface (SEI) film formation with electrolyte decomposition [45]. Recent study also revealed that the increase in interfacial resistance value which originates from parameters related to the electrode design such as thickness and density can cause capacity fading at higher rates [46]. It is also obvious from the figure that the cell restores its specific capacity again at 0.1C-rate from its 91st cycle indicating that the structural stability of the cathode materials retained.

Conclusions

Biodegradable and flexible egg shell membrane (ESM) was prepared and successfully employed as a separator for lithium-ion batteries. The ESM possesses higher porosity and exhibited better wettability than the commercial membrane. The ESM was thermally stable up to 240 °C and had better compatibility with lithium metal anode. Although, cell comprising ESM as separator delivered a discharge capacity of 60 mAhg⁻¹ at 1 C-rate with a stable cycling, concerning the inferior mechanical property in terms of its lower tensile strength and also its dimension would render large-scale production of such membranes somewhat difficult.

Acknowledgements

DAE- BRNS, Mumbai is gratefully acknowledged for financial support.

Address

*Electrochemical Power Sources Division, CSIR – Central Electrochemical Research Institute, Karaikudi, 630 006, India.

E-mail: arulmanuel@gmail.com; amstephan@cecri.res.in

References

- 1 J. M. Tarascon, M. Armand, Nature, 2001, **414**, 359
- 2 R. Bouchet, S. Maria, R. Meziane, A. Aboulaich, L. Lienafa, J. P. Bonnet, T.N.T. Phan, D. Bertin, D. Gignes, D. Devaux, R. Denoyel, M. Armand, Nat. Mater., 2013, **12**, 452
- 3 A. Manuel Stephan, Eur. Polym. J., 2006, **42**, 21
- 4 P.G. Balakrishnan, T. Prem Kumar, J. Power Sources, 2006, **155**, 401
- 5 P. Arora, Z. Zhang, Chem. Rev., 2004, **104**, 4419
- 6 X. Huang, J. Solid State Electrochem., 2011, **15**, 649
- 7 J. Y Song, Y Y Wang, C C Wan, J. Electrochem Soc 2000, **147**, 3219
- 8 H. Wang, H. Huang, S. L. Wunder, J. Electrochem. Soc., 200, **147**, 2853
- 9 Y. J. Hwang, K.S. Nahm, A. Manuel Stephan, J. Membr. Sci. 2008, **310**, 349
- 10 Y. Saito, H. Kataoka, A. Manuel Stephan, Macromolecules, 2001, **34**, 6955
- 11 Y.E. Miao, G.N. Zhu, H. Hou, Y.Y. Xia, T.Liu, J. Power Sources, 2013, **226**, 82
- 12 Y.S. Lee, Y.B. Jeong, D.W. Kim, J. Power Sources, 2010, **195**, 6197
- 13 N. Angulakshmi, A. Manuel Stephan, Electrochim. Acta., 2014, **127**, 167
- 14 Nunes-Pereira J, Lopes AC, Costa CM, Leones R, Silva MM, Lanceros-Mendez S, Electroanalysis, 2012, **24**, 2147
- 15 Nunes-Pereira J, Lopes AC, Costa CM, Rodrigues LC, Silva MM, Lanceros-Mendez S, J Electroanal Chem., 2013, **689**, 223
- 16 M. Raja, T. P. Kumar, G. Sanjeev, L.Zolin, C. Gerbaldi, A. Manuel Stephan, Ionics 2014, **20**, 943-948
- 17 M. Raja, N. Angulakshmi, S. Thomas, T. Prem Kumar, A. Manuel Stephan, J. Member. Sci., 2014, **471**, 103
- 18 A. Manuel Stephan, T. Perm Kumar, R. Ramesh, S. Thomas, S.K. Jeong, K. S. Nahm, Mater.Sci.Engg A., 2006, **430**, 132
- 19 V. Subramanian, C.Luo, A. M. Stephan, K. S. Nahm, S. Thomas, B. Wei, J. Phys. Chem C 2007, **111**, 7527
- 20 Chiappone, F. Bella, J.R. Nair, G. Meligrana, R. Bongiovanni, C.Gerbaldi Chem.Electrochem., 2014, **1**, 1350
- 21 B.Dyatkin, V.Presser, M.Heon, M.R. Lukatskaya, M.Beidaghi, Y.Gogotsi, ChemSusChem, 2013, **6**, 2269
- 22 D. Yang, L. Qi, J. Ma, J. Mater. Chem., 2003, **13**, 1119
- 23 D. Yang, L. Qi, J. Ma, Adv. Mater., 2002, **14**, 1543
- 24 A.Y. Maria Christy, M.R. Jisha, Ae Rhan Kim, Kee Suk Nahm, Dong Jin Yoo, E. K. Suh, T. Sri Devi Kumari, T. Prem Kumar, A. Manuel Stephan, Bull. Korean Chem. Soc., 2011, **32**, 1204-1208
- 25 Z. Li, L. Zhang, D. Mithin, Adv. Energy Mater., 2012, **2**, 431-437.
- 26 H. Yu, Q. Tang, J. Wu, Y. Lin, L. Fan, M. Huang, J. Lin, Y. Li, F. Yu, J. Power Sources, 2012, **206**, 463
- 27 F. Yi, Z. Guo, L. Zhang, J. Yu, Q. Li, Biomaterials, 2004, **25**, 4591
- 28 J. Dennis, D. Carrino, K. Yamashita, A. Caplan, Matrix Biol. 2000, **19**, 683
- 29 J. Evans, C. A. Vincent, P. G. Bruce, Polymer, 1987, **28**, 2324-2328.
- 30 C. Gerbaldi, J. R. Nair, G. Meligrana, R. Bongiovanni, S. Bodoardo, N. Penazzi, J. Appl. Electrochem., 2009, **39**, 2199.
- 31 S. S. Zhang, J. Power Sources, 2007, **164**, 351.
- 32 S. Bodoardo, C. Gerbaldi, G. Meligrana, A. Tuel, S. Enzo, N. Penazzi, Ionics, 2009, **15**, 19
- 33 G. Meligrana, C. Gerbaldi, A. Tuel, S. Bodoardo, N. Penazzi, Journal of Power Sources, 2006, **160**, 516
- 34 J.A. Choi, S.H. Kim, D.W. Kim, J. Power Sources, 2010, **195**, 6192

Journal Name

- 35 Q. Shi, M. Yu, M.W. Zhou, Y. Yan, C. Wan, J. Power Sources, 2002, **103**, 286
- 36 J. Xi, X. Qiu, J. Li, X. Tang, W. Zhu, L. Chen, J. Power Sources, 2006, **157**, 501
- 37 J. Chen, S. Wang, L. Ding, Y. Jiang, H. Wang, J. Memb. Sci. 2014, **461**, 22
- 38 L.Z. Fan, J. Maier, Electrochem. Commn., 2006,8,1753.
- 39 A. Fericola, F. Croce, B. Scrosati, T. Watanabe, H. Ohno, J. Power Sources, 2007, **174**, 342
- 40 Y. Zhu, S. Xiao, Y. Shi, Y. Yang, Y. Wu, J. Mater. Chem. A, 2013, **1**, 7790
- 41 Z. Jiang, B. Carroll, K.M. Abraham, Electrochim. Acta, 1997, **42**, 2667
- 42 A. Manuel Stephan, K.S. Nahm, T. Prem Kumar, M. Anbu Kulandainathan, G. Ravi, J. Wilson, J. Power Sources, 2006, **159**, 1316
- 43 G.B. Appetecchi, F. Croce, B. Scrosati, Electrochim. Acta, 1995, **40**, 991
- 44 S. Brutti, J. Hassoun, B. Scrosati, C.Y. Lin, H. Wu, H.W. Hsieh, J. Power Sources, 2012, **217**, 72
- 45 J.H. Kim, S.C. Woo, M.-S. Park, K.J. Kim, T. Yim, J.S. Kim, Y. J. Kim, J. Power Sources, 2013, **229**, 190.
- 46 N. Angulakshmi, S. Thomas, Jijeesh R. Nair, R. Bongiovanni, C. Gerbaldi, A. Manuel Stephan, J. Power Sources, 2013, **228**, 294-299